QJEGH

Research article

Quarterly Journal of Engineering Geology and Hydrogeology

https://doi.org/10.1144/qjegh2022-075 | Vol. 56 | 2023 | qjegh2022-075

Subaqueous landslides associated with historical road improvements in steep glaciated terrain, Loch Lomond, western Scotland

Andrew Finlayson[1]*, Nikhil Nedumpallile-Vasu[2], Gareth Carter[1], Nicola Dakin[1] and Rhys Cooper[1]

[1] British Geological Survey, Lyell Centre, Research Avenue South, Edinburgh EH14 4AP, UK
[2] British Geological Survey, Environmental Science Centre, Nicker Hill, Keyworth, Nottingham NG12 5GG, UK
AF, 0000-0002-6447-3187
* Correspondence: afin@bgs.ac.uk

Abstract: Shorelines in steep glaciated terrain are focal points for development and can provide important natural corridors for transport (e.g. road, rail). However, the steep subaqueous slopes at nearshore sites present challenging ground conditions, and only in recent decades has the acquisition of continuous high-resolution bathymetric datasets become available to inform investigations. This study investigates a site in Loch Lomond, Scotland, where a reported displacement of 15 000 m^3 of rock fill occurred prior to completion and stabilization of an embankment for the A82 road, during improvement work undertaken in the 1980s. We revisit the area using new multibeam swath bathymetry, shallow sub-bottom seismic data and geomorphological mapping, as well as borehole logs from the original ground investigation. The bathymetric and seismic data provide strong evidence for older subaqueous landslide activity at the site. The data indicate that embankment construction was also associated with occurrence of subaqueous landslides, incorporating a total volume of up to 95 000 m^3. The research demonstrates the value of nearshore geophysical datasets in steep glaciated terrain, both for understanding geomorphological response to past shoreline modifications and as part of investigations where future developments (e.g. transport, energy infrastructure) are planned.

Received 29 July 2022; **revised** 6 February 2023; **accepted** 16 February 2023

The glaciated topography of the western Scottish Highlands exhibits a large number of inland lochs occupying ice-carved basins and an irregular coastline deeply indented by sea lochs (fjords). The shorelines of these waterbodies now provide locations for a range of developments and form important natural corridors that are used by strategic transport routes to pass through high-relief terrain. Over recent decades there has been a focus on improving road standards along a number of lochside routes, with the objective of reducing congestion and accident severity rates (Transport Scotland 2009). There is also wider recognition that the strategic road network in steep environments needs to be resilient to climate change and related hazards (Transport Scotland 2016).

Lochside locations can present challenging ground conditions for infrastructure development such as transport improvement, particularly where steep valley sides and subaqueous loch slopes leave limited space for route widening. Engineering solutions may include creating road cuttings into valley sides or extending embankments or viaducts out from the shoreline. Examination of terrestrial datasets (e.g. aerial photographs and digital terrain models) forms a key stage in the geological assessment of slopes above such sites. However, it is only in the last couple of decades that tools have become widely available to capture continuous high-resolution bathymetric information from subaqueous slopes below them (Chiocci *et al.* 2011). Multibeam swath bathymetry and shallow sub-bottom seismic imaging techniques are routinely used in seabed geomorphological mapping and geohazard assessment for offshore sites (Hough *et al.* 2011), and are now increasingly being used for landfall locations for cables and pipelines. Recent studies have used these approaches to investigate subaqueous geomorphological processes in nearshore coastal and inland waterbodies (e.g. Stoker *et al.* 2010; Lowag *et al.* 2012; Miller *et al.* 2013; Pinson *et al.* 2013; Carter *et al.* 2020) with the resulting datasets providing valuable evidence relating to past slope activity, sometimes at a greater level of detail than adjacent onshore sites where the land surface may be masked by forest or modified by land use (e.g. agriculture).

There is now an excellent opportunity to use new bathymetric datasets to examine steep nearshore subaqueous slopes adjacent to shorelines that have been modified by historical lochside development. Understanding the interaction between past engineering constructions and the subaqueous slopes in these settings will add to a knowledge base that could help inform and improve planning for new schemes (e.g. L'Heureux *et al.* 2010). This may be especially important where possible risks (to people or to other loch bed infrastructure, such as cables or pipelines) may be posed by geomorphological processes directly arising from the shoreline modifications.

In this study we use an example of two deepwater embankments constructed in the 1980s during improvement of the A82 Loch Lomondside road, at a site known as Wades Bridge Bank (Fig. 1). A report following the construction described displacements of natural soil and rockfill, including the unexpected movement of an estimated 15 000 m^3 of fill at the southernmost embankment, prior to completion and subsequent work on the new road (Howison and MacDonald 1988). At the time survey techniques were not available to examine the extent or wider impact of any subaqueous landslide activity on the loch bed resulting from the embankment displacements. The research described here revisits the Wades Bridge Bank site, combining recently collected multibeam swath bathymetry, shallow sub-bottom seismic data, geomorphological mapping and the original ground investigation borehole logs, to understand the impact of the embankments on the subaqueous landscape. The specific aims are to (1) investigate the site's geomorphological context using the newly available data,

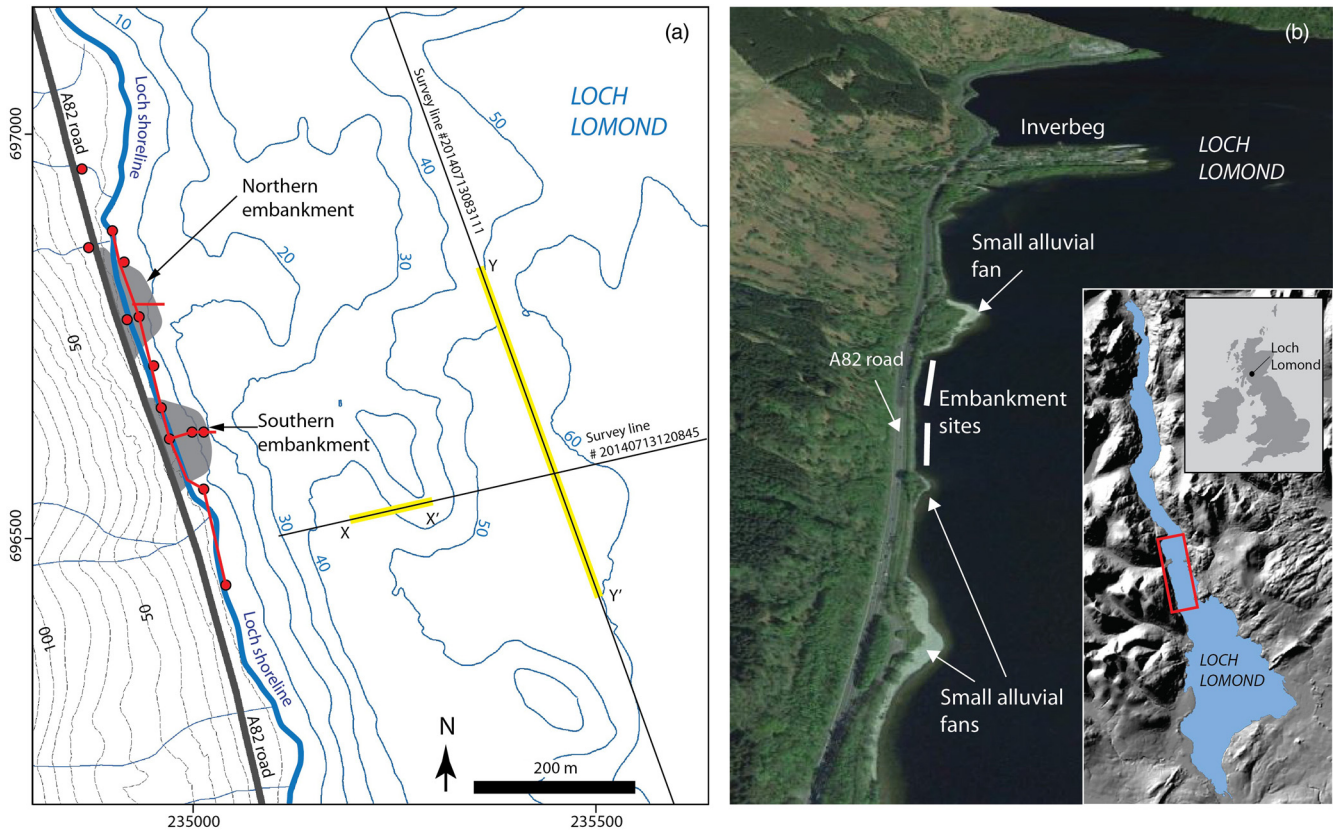

Fig. 1. (**a**) Map of study area showing A82 road, the position of the Wades Bridge Bank deepwater embankments and the Loch Lomond shoreline. The locations of boreholes consulted in this work are shown in red (these were drilled prior to embankment construction), and the positions of the cross-section lines in Figure 11 are shown in red. The locations of the seismic lines in Figures 6 and 8 are shown in yellow. Elevation contours (black) and water depth contours (blue) are shown in 10 m intervals. (**b**) Oblique aerial view showing context of study area. © 2022 Landsat/Copernicus Image, source: Google Earth. Inset: red box shows location of site along the western shore of Loch Lomond. Hill-shaded surface model build from Intermap Technologies NEXTMap Britain elevation data.

(2) describe the nature and extent of subaqueous landslides associated with displacements at the embankments, (3) explore whether older Holocene slope failures may have occurred at the site, indicating a pre-existing susceptibility in the area, and (4) reconstruct the possible evolution of the southern embankment failure using runout modelling. The paper goes on to consider how these data and interpretations add new insight to subaqueous slope processes at the site, which could be of relevance for developing conceptual models in similar steep nearshore terrain.

Background

Geological setting

Loch Lomond is Britain's largest freshwater body by area (71 km^2) and is located in the southwestern Scottish Highlands. The loch currently has an average water level of *c.* 8 m above Ordnance Datum (OD) (SEPA 2022). The Wades Bridge Bank deepwater embankments are located on the western shore of the loch, 1.3 km to the south of a prominent delta at Inverbeg (Fig. 1b). The local bedrock geology consists of Neoproterozoic metasandstones (psammites) and metasiltstones (semipelites) belonging to the Beinn Bheula Schist Formation of the Southern Highland Group. In the vicinity of the site these rocks form part of the Highland Border Steep Belt and possess a foliation that dips towards the SSE at angles of 60–70° (BGS 1987; Stephenson and Gould 1995). Locally these rocks are intruded by ENE-trending quartz-dolerite dykes of Carboniferous age and a lamprophyre dyke (formerly quarried above the A82 road) of Early Devonian age.

Loch Lomond itself is a glacially eroded basin that was last occupied by ice during the Loch Lomond Stadial, *c.* 12.9–11.7 ka BP. At that time, a southward flowing outlet glacier advanced through the loch and beyond the southern shore leaving deposits of subglacial till, moraines and glaciofluvial outwash that have been investigated at several onshore localities (e.g. Rose *et al.* 1988). Final glacier retreat in Loch Lomond is suggested to have occurred very near the end of the Stadial and close to the onset of the Holocene (MacLeod *et al.* 2011). During the early to mid-Holocene a short-lived rise in relative sea-level to *c.* 12 m OD temporarily connected Loch Lomond to the sea (Dickson *et al.* 1978). Fragments of raised shoreline from this episode are present at several locations around the loch, including near Wades Bridge Bank. Continued isostatic rebound then elevated the land surface, restoring the loch to its current freshwater condition.

The slopes above the Wades Bridge Bank site rise steeply at angles of between 20 and 40° to an elevation of *c.* 300 m OD, before continuing more gently up to the summit of Beinn Dubh to the west (642 m). Bedrock is generally close to the surface (and exposed at surface in places) with a thin cover of colluvial soils. Immediately to the north and south of the embankments, small alluvial fans protrude from the loch shore (Fig. 1b). Away from the fans, the shoreline in this part of the loch largely consists of riprap boulders placed as shore protection measures (Hansom and McGlashan 2000).

There are sparse descriptions of the loch bed sediments in Loch Lomond. Farmer and Lovell (1986) collected a number of short sediment cores from water depths >20 m, describing the top 20 cm to range from highly porous brown muds to black micaceous oozes.

Dickson *et al.* (1978) and Turner and Thompson (1979) investigated a *c.* 5 m long Holocene sequence recovered from a core in the southern Loch Lomond basin, *c.* 8 km to the SSW of the Wades Bridge Bank site. The material generally comprised organic brown silty clay or 'gyttja' (fine-grained organic-rich lacustrine soil) with a brackish-water mud (relating to the marine phase) between 3 and 4 m depth, but the core did not penetrate any of the underlying material. In the vicinity of Wades Bridge Bank, shallow water borehole logs associated with the A82 road improvement work contain some descriptions of the subaqueous loch slope soils (discussed in the section on geomorphological context below).

The Wades Bridge Bank deepwater embankments

Descriptions of the Wades Bridge Bank deepwater embankments have been given by Howison and MacDonald (1988, 1989) and are briefly summarized here. The site consists of a northern and southern embankment (Fig. 1a), each *c.* 100 m in length, which are split by a small rock headland. Prior to construction, site investigation results were interpreted to suggest that sands and gravels were present at the loch bed on the nearshore slope, overlying a layer of soft organic soil, which in turn rested on dense sands and gravels at depth. About halfway down the slope the organic soils appeared to come to the loch bed surface. The design considered that displacement of the organic material was not likely to occur, owing to the overlying sands and gravels on the upper slope, and therefore aimed for containment of material upon placement of fill, and improvement of shear strength with time. The construction was to involve placement of an initial toe bund, following which layers of rockfill were placed from the base of the embankment to the top. At the northern embankment, placement of the toe bund was accompanied by penetration into, and displacement of, some loch bed material after which subsequent rockfill layers were set down as expected. However, as the bulk of underwater placement was nearing completion at the southern embankment, monitoring indicated that a major displacement had occurred moving *c.* 15 000 m^3 of rock fill downslope. Filling then resumed with subsequent emplacement proceeding steadily to the surface and monitoring indicating stabilization of the embankment.

Datasets and methods

Datasets

This study utilizes loch depth data that were collected during a swath bathymetry survey of the entirety of Loch Lomond, carried out between November 2007 and February 2008, *c.* 20 years after the completion of the embankments. The survey used the British Geological Survey (BGS) multibeam system mounted on the Loch Lomond and Trossachs National Park's (LLTNP) solar powered catamaran, the *Bata Greine*. Because of the loch bed gradient, minimum water depths that could be surveyed in the vicinity of the site were *c.* 4 m. Bathymetric and backscatter (a measure of the acoustic signal return strength) data were output in the form of *xyz* grid data at 2 m horizontal resolution and converted into ascii files for visualization and interpretation in ArcGIS and GoCad-SKUA software. Derivative grids including hillshade, slope and curvature were generated from the loch bathymetic data to aid interpretation (Fig. 2). Onshore, NEXTMap Britain digital elevation data (5 m horizonal resolution) and georeferenced colour aerial photographs were used to investigate the surface morphology around the embankments.

Seismic reflection data were captured in July 2014 using an EdgeTech 3100 portable sub-bottom profiling system towed from the BGS *White Ribbon* survey boat. The position of survey lines within the area of interest for this study are shown in Figure 1a. The seismic lines were examined for evidence of recent subaqueous landslides at the loch bed and also for older landslide deposits buried below the surface.

Logs from boreholes drilled in 1982, as part of the ground investigation works for the A82 road upgrade, provided information about the nature of soils and ground conditions prior to the construction of the embankments (these borehole records are viewable in the BGS Onshore GeoIndex: https://www.bgs.ac.uk/map-viewers/geoindex-onshore/). The loch bed elevations in the borehole records also provided information about the pre-embankment loch bed surface profile. The locations of boreholes used in this study are shown in Figure 1a.

Geomorphological analysis

Desk-based geomorphological mapping was undertaken in ArcGIS, during which the datasets were examined in order to interpret the shallow geology at and around the site. A walk-over survey along the shoreline section of the site was also undertaken to supplement the desk-based investigation. The bathymetric data were examined to interpret the subaqueous extent of the embankments and to identify features indicative of landslides on the loch bed. Morphometric parameters for the subaqueous landslides were captured according to the approach outlined by Clare *et al.* (2019).

A pre-embankment loch bed surface model was generated following the approach described by Carter *et al.* (2020) and used to estimate the depth of erosion and deposition associated with landslides downslope from the embankments. This approach consisted of removing the area within the interpreted embankment and associated landslide footprint from the swath bathymetry dataset. Contours were then manually connected across those areas following the observed general trend of the loch bed surface outside the landslide footprint, and these were used to interpolate an estimated pre-failure surface. There is a degree of subjectivity in this process, with difficulty in quantifying error being acknowledged as a shortcoming. However, closer to the shore the loch bed elevations recorded in the pre-embankment boreholes provided useful surface constraint.

Subaqueous landslide runout modelling

Runout modelling for subaqueous landslide activity associated with the main southern embankment displacement (Howison and MacDonald 1988) was performed using the single-phase RAMMS (Rapid Mass Movement Simulation) model developed by the WSL Institute for Snow and Avalanche Research SLF. The model uses a depth-averaged shallow water equation derived from the first principles of mass and momentum conservation (Christen *et al.* 2010) and employs Voellmy-fluid friction type rheology (equation 1)

$$S = \mu N + \frac{\rho g u^2}{\xi} \tag{1}$$

and

$$N = \rho h g \cos(\phi) \tag{2}$$

where ρ is the density, μ is the friction coefficient, g is the gravitational acceleration, ϕ is the slope angle, h is the flow height, u is the flow velocity and ξ is the turbulence coefficient. The Voellmy model accounts for the resistance of the solid phase controlling the flow behaviour (μ) and a viscous or turbulent fluid phase influencing the flow velocity (ξ). RAMMS also has a modified Voellmy equation (equation 3) to incorporate yield stress to account for non-linearity exhibited by materials such as lacustrine muds

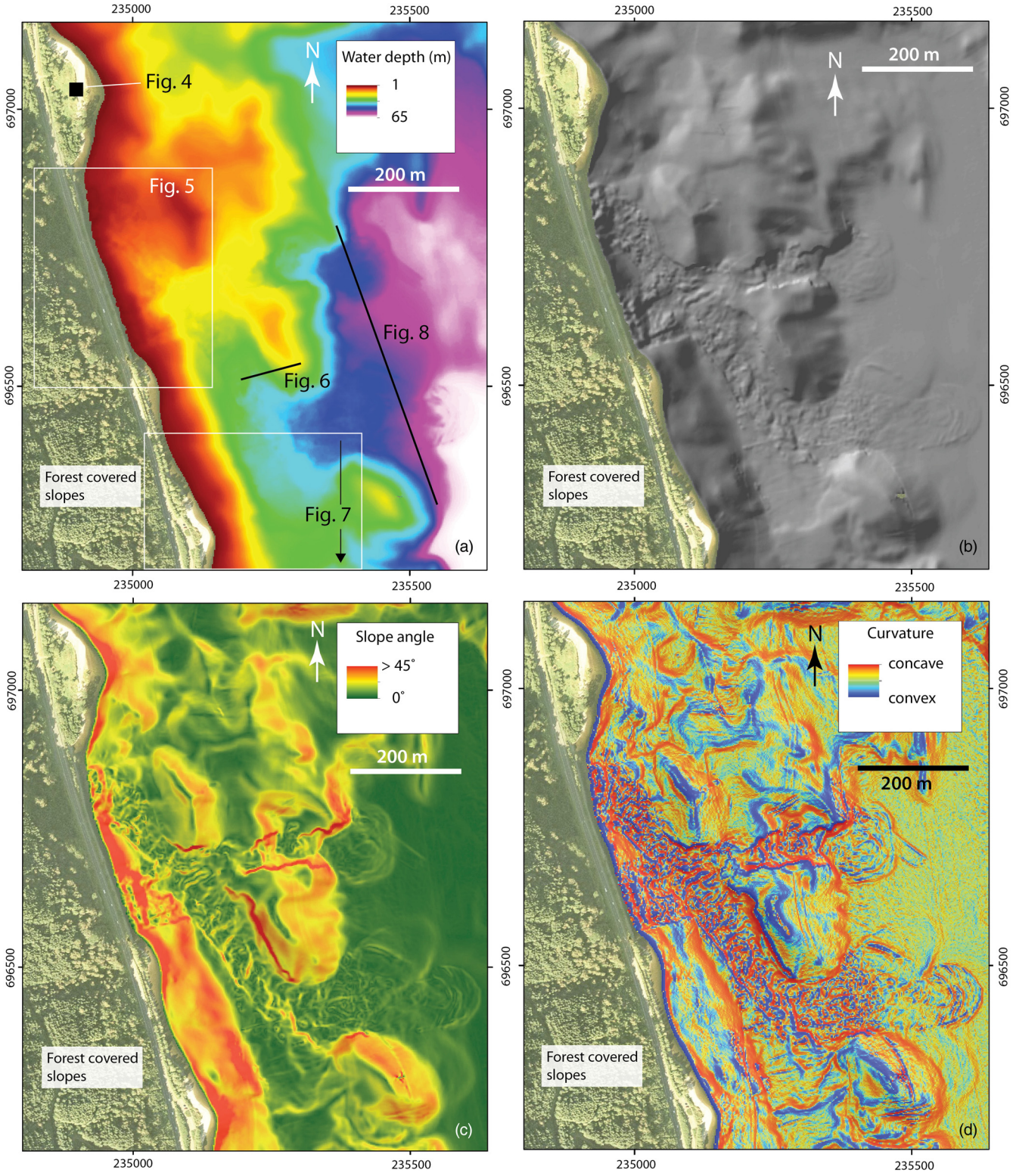

Fig. 2. Multibeam data and derivatives showing (**a**) water depth, (**b**) hill-shaded relief with NW illumination, (**c**) slope angle and (**d**) curvature. Aerial photograph © Getmapping: Licence Number UKP2006/01.

(referred to as Voellmy-cohesion in this paper)

$$S = \mu N + \frac{\rho g u^2}{\xi} + (1-\mu)N_0 - (1-\mu)N_0 e^{-N/N_0} \qquad (3)$$

where N_0 is the yield stress of the flowing material and μ is the hardening parameter. Depending on N_0, the model increases the shear stress and therefore causes the landslide to stop earlier.

RAMMS integrates an entrainment module to estimate the eroded depth and volume during landslide runout. Selections from pre-defined values were made for the estimation of three parameters: potential erosion depth, erosion rate and critical shear stress. The potential erosion depth parameter controls the depth of maximum potential erosion as a function of shear stress, varying from 0.05 to *c.* 0.2 m kPa^{-1}. The erosion rate parameter determines the rate at which different materials are entrained, ranging from 0.013 m s^{-1} for densely packed soils to 0.05 m s^{-1} for loose soils. The third

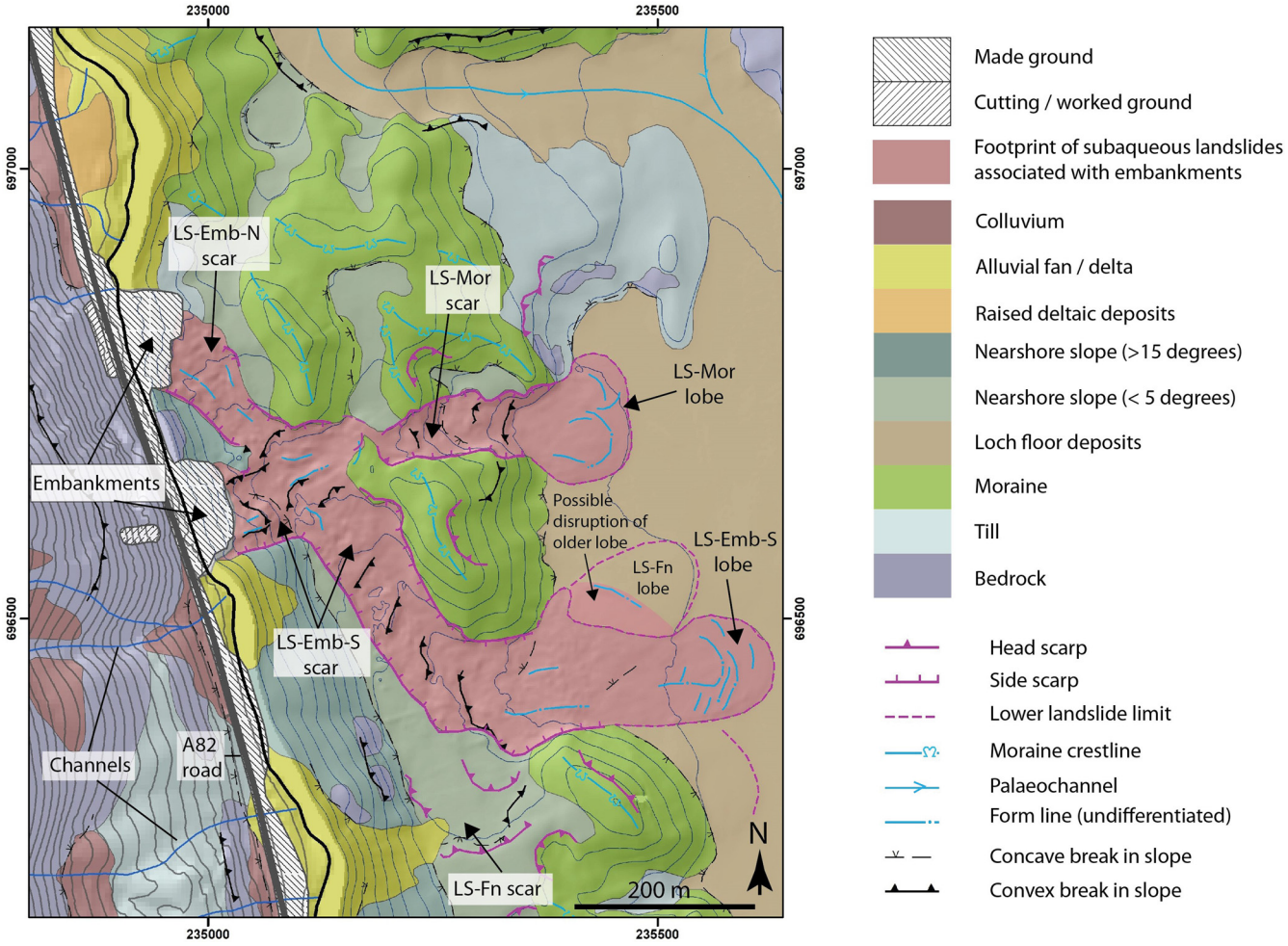

Fig. 3. Geomorphological map of study area showing surface geology and the footprint of subaqueous landslides that can be traced upslope to the embankments. LS-Emb-N, northern embankment landslide; LS-Emb-S, southern embankment landslide; LS-Mor, moraine landslide; LS-Fn, fan edge landslide.

parameter, critical shear stress, controls the initiation of erosion during the flow, where lower values suggest the bed to comprise materials that are relatively easy to erode. The built-in parameter values within RAMMS have generally been developed based on a subaerial context (Berger *et al.* 2011; Schürch *et al.* 2011; Frank *et al.* 2017), and therefore this study also represents an exploration of their applicability and transferability in a subaqueous setting. Further detail on model calibration and input information derived from the geomorphological investigation is given in the results section.

Results

Geomorphological context

A map of the geomorphology and interpreted superficial geology at the site is shown in Figure 3, and the general setting is described here from west to east as higher to lower elevation, respectively. Onshore, the slopes above the road are mapped as bedrock near the surface with thicker patches of colluvium present in slope concavities. Drainage channels are spaced *c.* 100–200 m apart except for the area above the embankments, where a slight rock buttress diverts drainage to the north and south. Small alluvial fans with beaches extend out from the shoreline to the north and south of the embankments, where the fluvial channels enter the loch. The centre of the larger fan immediately to the north of the embankments is formed around a partially eroded raised delta surface, graded to 12 m above OD and comprising medium dense, dipping foreset sands and gravels (Fig. 4). This is probably a remnant feature from the Holocene relative sea-level highstand when marine waters temporarily entered Loch Lomond between *c.* 7000 and 5500 years ago (Dickson *et al.* 1978). Boreholes from the edges of the fans recorded loose gravels at the surface overlying silty sand and gravel, which becomes dense to very dense with depth, with total soil thickness exceeding 10 m. A characteristic of the fans is the presence of buried soft organic soil units. These layers may have become buried through processes such as channel switching (avulsion) and overtopping during higher energy discharge events, or local erosion and redistribution of raised beach or delta deposits (e.g. recently collapsed material in Fig. 4). Between the embankments, bedrock has been mapped at surface and was recorded as moderately strong to strong schistose phyllite with 70° dipping foliation at the loch bed level in a borehole log (A82 Luss to Tarbet Borehole number 460).

Artificial ground (road surface and riprap boulders) masks much of the underlying geology along the shoreline edge of the embankments. However, the pre-embankment ground investigation boreholes indicate that a sequence, up to 5 m in thickness, of medium dense to very dense gravels with cobbles was recorded there. These soils are likely to have been originally derived from colluvium or glacial till at the shore, with finer material having been washed out by wave action.

The natural loch bed surface slopes down from the shore at angles of 20–35° in the nearshore area. Two boreholes drilled prior to the

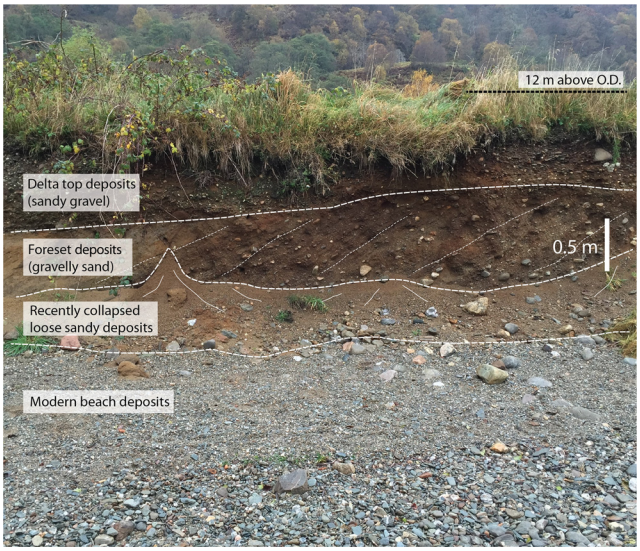

Fig. 4. Sediments contained within the eroded delta at the fan or beach immediately to the north of the northern embankment. The surface of the feature is graded to 12 m OD and probably relates to an elevated loch level when seawater last entered Loch Lomond during the Holocene sea-level highstand, between 7000 and 5500 years ago. (Note recently collapsed, loose sandy deposits at the cliff base indicating continuing sediment reworking.)

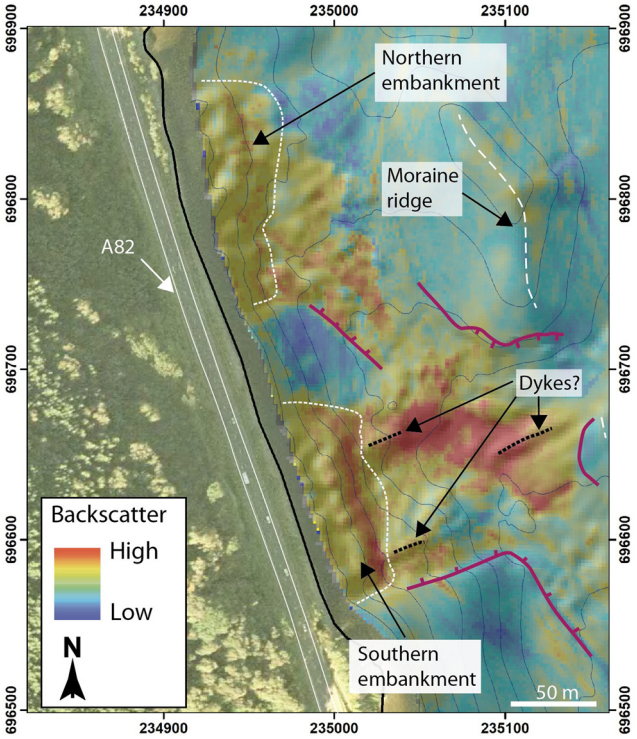

Fig. 5. Backscatter data (with slight transparency applied) draped over hill-shaded relief image (NW illumination). Red colours represent higher strength return. The embankment outlines are marked by breaks in slope and strong backscatter return consistent with a rockfill texture at surface. Aerial photograph © Getmapping: Licence Number UKP2006/01.

embankment construction and located between 30 and 40 m away from the shore recorded 2.5–3.0 m of soft silty and clayey organic soil at the surface of the loch bed slope. These organic silts and clays overlie medium dense silty sand, becoming increasingly gravelly and dense with depth, before boulders or rockhead were encountered at 5.0–7.0 m depth below the loch bed.

There is a break in slope at *c.* 100 m from the shore where the gradient of the nearshore slope reduces to less than 5°, beyond which a prominent SSE-trending ridge is encountered before the loch bed reaches the local basin floor at 60 m water depth. The ridge is interpreted as a moraine, relating to an ice-marginal position of the Loch Lomond glacier as it retreated at the end of the Loch Lomond Stadial, *c.* 11 700 years ago (MacLeod *et al.* 2011).

Subaqueous landslide morphology

The spatial extents of the final embankments are identified by the bathymetric breaks in slope combined with a strong return in the backscatter, as would be expected from a boulder fill surface (Fig. 5). These align with the planned extent of the two embankments shown on original site investigation documents. Two clear subaqueous landslide scars, characterized by side scarps and a rugose surface, extend downslope from each of the embankments (Figs 2 and 3). The precise location and height of the head scarps for these slides could not be identified owing to masking by the final embankment fill.

The northern embankment landslide (named here LS-Emb-N) follows a SSE direction where it has been focused along the shoreward side of the moraine ridge a short distance downslope from the embankment. The scar width reaches 97 m across below the embankment but then narrows to *c.* 50 m. Approximately 150 m downslope from the northern embankment the scar is crosscut and obscured by the scar of the southern embankment landslide (LS-Emb-S, Figs 3 and 5).

The LS-Emb-S scar initially follows the steep eastward-facing nearshore slope before turning SSE at the break in slope, where it is diverted along a gentler gradient down the shoreward side of the moraine ridge (Fig. 3). There is a distinct area with a strong backscatter return where the LS-Emb-S landslide scar cuts the LS-Emb-N scar (Fig. 5). This area is also characterized by broad ENE-trending ridges with a similar alignment and position to dykes mapped onshore, suggesting that the backscatter here may also reflect where soil has locally been eroded to reveal bedrock. Further downslope, a seismic profile shows the side scarp cutting stratified Holocene soils at the loch bed surface (Fig. 6). These Holocene soils rest on the glacier moraine, for which the internal structure could not be resolved by the chirp data. There is no subsequent deposition draping the side scarp edge, indicating that it is recent and does not relate to an earlier Holocene failure. The bathymetry indicates that the height of the side scarp at this location is *c.* 3.5 m. A poorly defined chaotic unit with a rugose upper surface is present at the base of the side scarp, suggesting the presence of disturbed and transported infill material. Approximately 400 m downslope from the embankment, the LS-Emb-S landslide is directed eastward once more, with some debris appearing to overtop the main channel at the southern bend, before continuing towards the depositional zone at the loch floor level (60 m water depth). The LS-Emb-S landslide scar reaches 115 m in width and maintains a width of at least 85 m for most of its 475 m evacuation length. The depositional lobe extends a further 255 m with a surface that sits *c.* 1.8 m above the loch floor and is characterized by arcuate features interpreted as compressional ridges at its distal end (Fig. 3). This lobe appears to have been directed partially through, and to the south of, another pre-existing smoother depositional lobe (described below).

A third landslide, with a similar rugose surface expression to the embankment landslides, is located on the eastern slope of the moraine (Figs 2 and 3) and is referred to here as the moraine landslide (LS-Mor). The headscarp is 2.0–4.0 m high and is located near the top of the moraine where some debris from one (or both) of the embankment landslides appears to have overtopped the ridge, potentially destabilizing material mantling the moraine slope. The LS-Mor landslide has an evacuation length of 173 m and

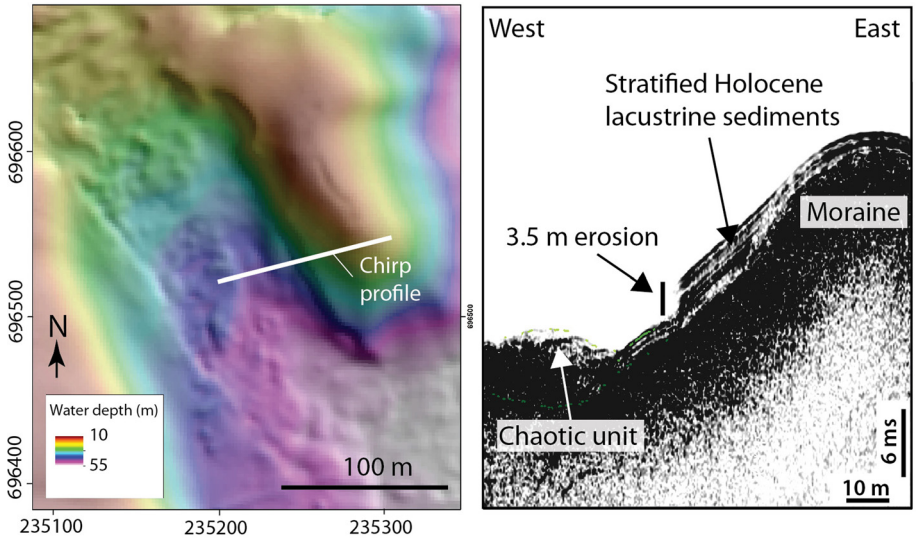

Fig. 6. Chirp profile across the southern embankment landslide scar showing the side scarp cutting stratified sediments that drape the moraine ridge. Vertical scale is in milliseconds two-way-travel time (TWT).

depositional lobe that is 138 m long. The surface of the depositional lobe forms a positive bathymetric feature *c.* 2.2 m above the surrounding loch floor and possesses compressional ridges towards the toe of the deposit.

There are a number of additional subaqueous landslide features in the area that exhibit a more subdued surface expression. A scar and relatively well-defined evacuation zone are apparent to the south of the LS-Emb-S landslide path at the foot of the steep nearshore slope, where the geomorphology suggests the presence of an apron of soil that is fed from the fan or delta above (Fig. 3). This landslide is referred to as the fan-edge landslide (LS-Fn) and possesses a 3–4 m high headscarp. The interpretation of focused soil loading from the fan above is supported by the strong backscatter return suggesting localized deposition of coarser grained material at this location (Fig. 7). The scar is broadly oriented towards the NE and appears to align with the smooth lobe on the loch floor that has been overtopped, and possibly further disrupted, by the chronologically later LS-Emb-S landslide lobe (Fig. 3). The seismic line Y–Y' shows a chaotic unit that corresponds to the rugose surface of the LS-Emb-S landslide lobe and also extends towards the ridge that is developed in the smoother (partially overridden) lobe (Fig. 8). This surface chaotic unit overlies a lower chaotic unit that is interpreted as a deposit from the older LS-Fn landslide. A third, distinct body of chaotic reflectors is also present at depth under the southern lobe, close to the base of the stratified (Holocene) seismic facies. This unit is separated from the upper chaotic units by strong bedded reflectors and must therefore relate to an older event.

Breaks in slope also suggest somewhat smoother scars immediately surrounding the area of the moraine landslide (LS-Mor) (Fig. 3). There is no depositional lobe morphology directly associated with these features visible in the multibeam bathymetry; however, the seismic line shows at least one buried unit of chaotic reflectors, which sits underneath and is separate from a surface unit of chaotic reflectors corresponding to the LS-Mor landslide lobe (Fig. 8).

Interpreting the sequence of subaqueous landslides

Three main groups of landslide features have been interpreted (Fig. 9).

Group A: earlier Holocene landslides

Group A features include a number of scars that are relatively smooth in appearance, suggesting that they now possess a drape of chronologically more recent loch bed soil and/or slope modification has occurred over the intervening time between initial failure and the present day (e.g. localized slumping of the steepest segments of headscarp). These features generally have no visible associated depositional lobes or can be tentatively linked with the buried lobes that occur within and near the base of the stratified Holocene seismic unit (Fig. 8). The Group A features are interpreted as having occurred earliest and may relate to post-glacial or early to mid-Holocene mass movements.

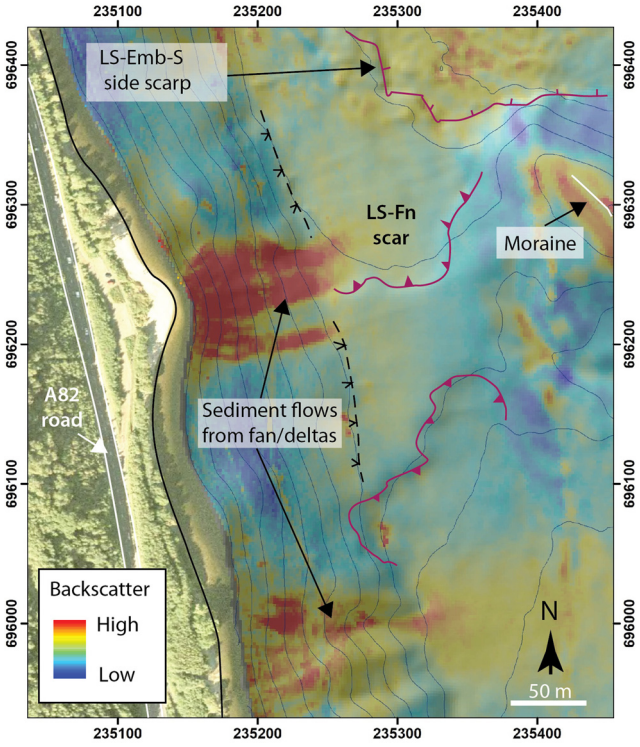

Fig. 7. Backscatter data (with slight transparency applied) draped over hill-shaded relief image (NW illumination). Red colours represent higher strength return. Backscatter suggests coarser-grained sediment flows from the alluvial fan being transported to the lower gradient nearshore slope below. The areas of localized loading correspond to more subdued (older) head scarps. Aerial photograph © Getmapping: Licence Number UKP2006/01.

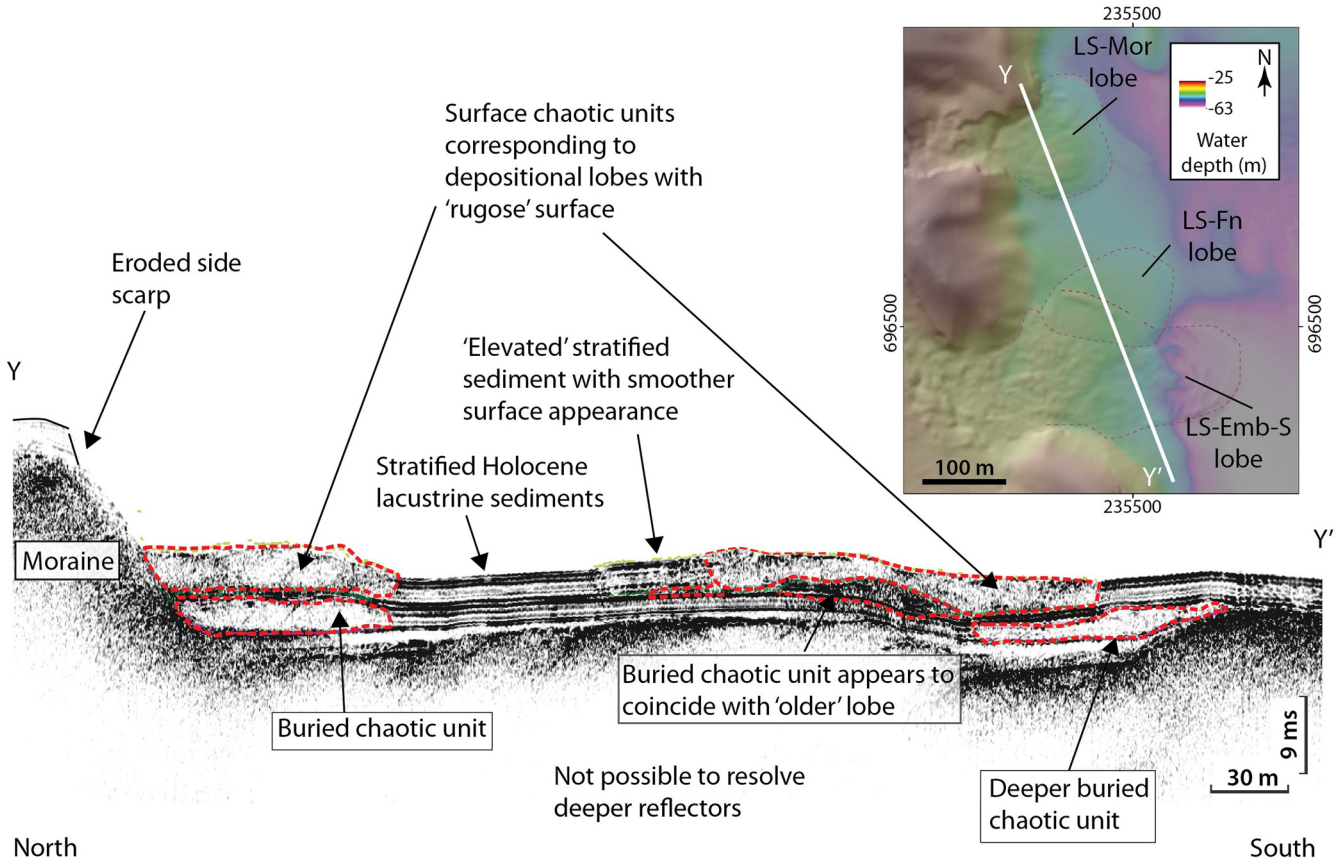

Fig. 8. Chirp profile showing both surface and buried units characterized by weak chaotic reflections. The surface units correspond to the landslide depositional lobes that can be clearly seen in the multibeam imagery. Vertical scale is in milliseconds two-way-travel time (TWT).

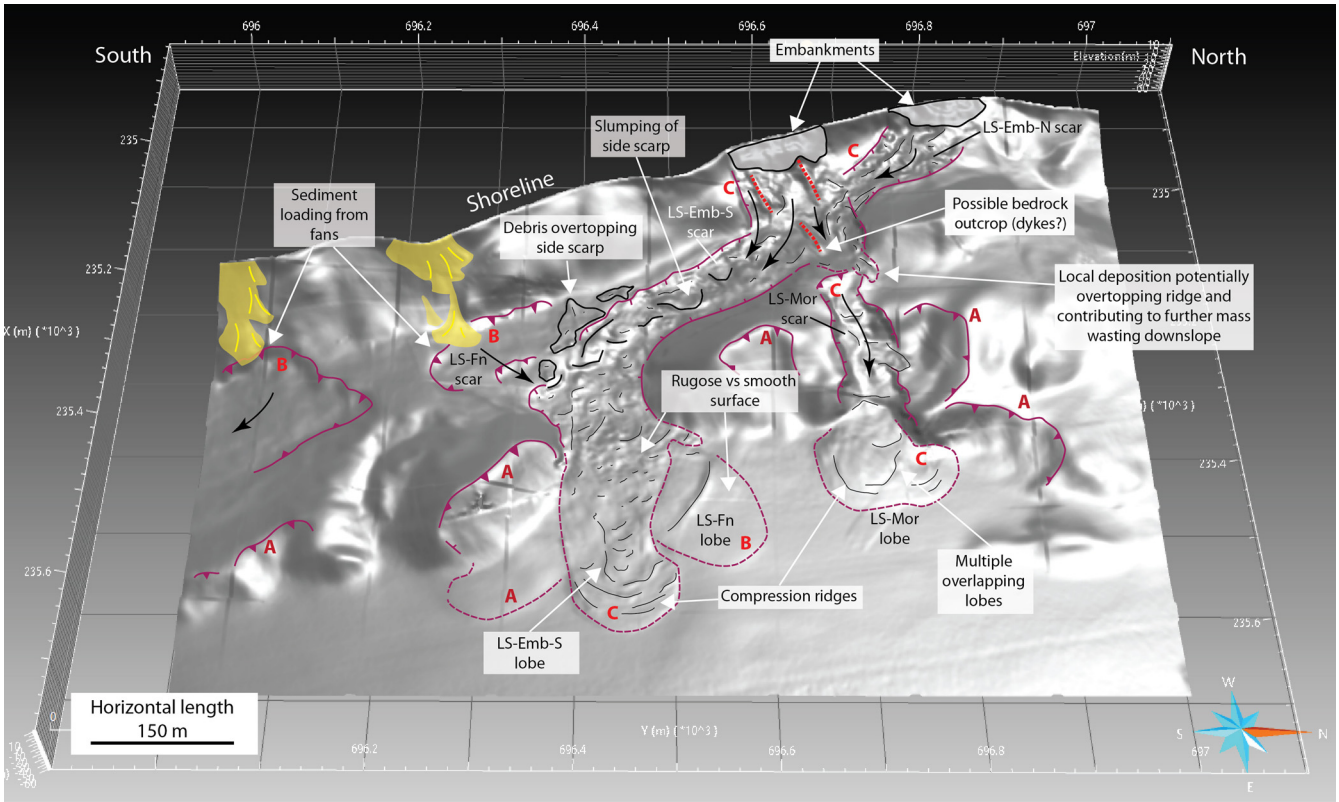

Fig. 9. Oblique view looking towards the west showing conceptual sequence of subaqueous landslides. Group A, earlier Holocene landslides; Group B: landslides potentially associated with loading from alluvial fans; Group C: landslides associated with embankment construction.

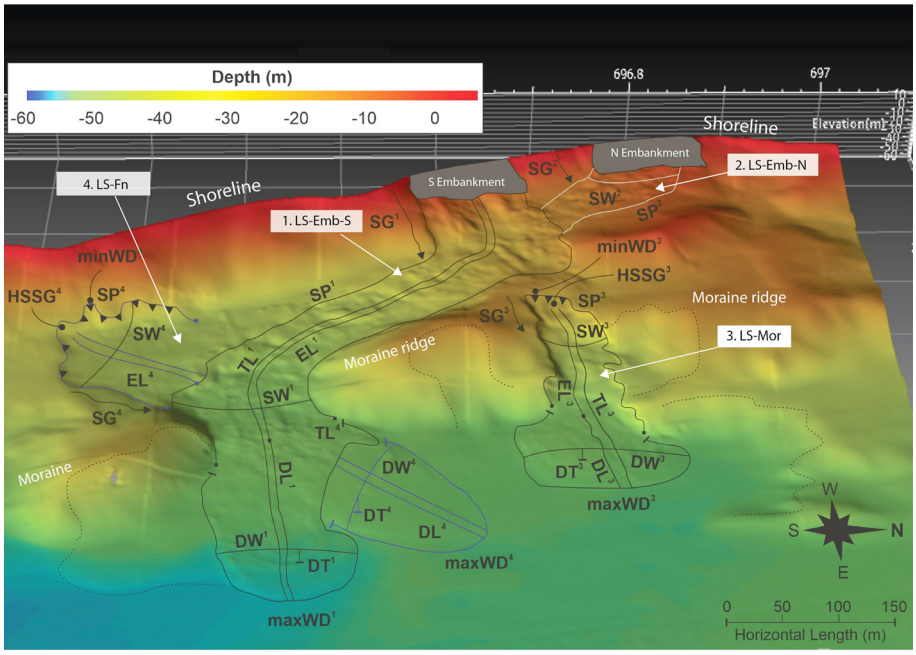

Fig. 10. Morphometric parameters measured for four of the subaqueous landslides. Abbreviations and values are given in Table 1.

Group B: landslides potentially associated with loading from alluvial fans

Group B features also include relatively smooth landslide scars, suggesting a degree of subsequent sedimentation or modification of the edges. However, the location of these scars coincides with zones where soil loading from shoreline fans is evident (Figs 7 and 9). Sedimentation from the fans above is still a continuing process; therefore, these scars are considered potentially more recent than the Group A features. This interpretation is also supported by the visibility (albeit smoother in appearance) of the partially overridden Group B lobe, which can be traced to the north of the LS-Emb-S landslide lobe (Fig. 9) and forms a continuation from the fan-edge landslide (LS-Fn) scar.

Group C: landslides associated with embankment construction

Group C features possess characteristically more rugose surfaces, which have not been subjected to burial by subsequent significant sedimentation. These features are attributed to the emplacement of the embankments. We interpret the northern embankment landslide (LS-Emb-N) to have occurred first. The extent of this landslide is not known; however, it is noted that no significant movements were detected by monitoring at that location (Howison and MacDonald 1988). The large southern embankment landslide then occurred (as detected by monitoring at the time), resulting in local erosion down to bedrock and development of a wide scar below the LS-Emb-S onset area (Fig. 5). Overtopping of the moraine ridge from either the LS-Emb-N or LS-Emb-S landslide could have caused loading on the convex slope at the crest, possibly acting as a trigger for the moraine landslide (LS-Mor), which is also interpreted as part the Group C events.

Using these interpretations, the morphometric parameters for the LS-Emb-N, LS-Emb-S, LS-Mor (all Group C) and LS-Fn (Group B) landslides were recorded (Fig. 10, Table 1). Measurements for the other earlier features could not be made as their morphology could not be accurately defined and quantitative values could potentially be misleading owing to subsequent slope modification.

Pre-embankment geomorphological context and surface change

The estimated loch bed surface prior to embankment construction and occurrence of the Group C landslides is shown in Figure 11, alongside a fence diagram with the interpreted simplified geology

Table 1. *Summary of morphometric parameters for four subaqueous landslides at Wade's Bridge Bank, Loch Lomond*

	1. LS-Emb-S	2. LS-Emb-N	3. LS-Mor	4. LS-Fn
Minimum water depth (minWD)	Null	Null	30.5	29
Maximum water depth (maxWD)	63	Null	61	61
Scar perimeter (SP)	1192	425	444	353
Scar width (SW)	115	97	64	93
Evacuation length (EL)	475	Null	173	105
Deposit length (DL)	255	Null	138	333
Total length (TL)	728	Null	311	439
Deposit width (DW)	120	Null	148	130
Deposit thickness above loch floor (DT)	1.8	Null	2.2	2.0
Slope gradient (SG)	30.5	41.5	8.5	6.0
Headscarp slope gradient (HSSG)	Null	Null	12.5	11.5

All metrics are measured in metres except gradients (degrees). Water depths are given in metres below loch level. In Figure 10, landslide number is denoted by superscript numbers next to metric abbreviations; for instance, evacuation length for Slide 1 (LS-Emb-S) is shown as EL^1. The scar perimeter value for LS-Emb-N (SP^2 in Fig. 10) represents only the portion of the scar that can be categorically attributed to the LS-Emb-N landslide, as this scar has been affected by subsequent events, meaning that this value may be an underestimation of true scar perimeter (SP) length. For the same reason, many metrics for LS-Emb-N are Null as these features cannot be measured with any degree of confidence. Similarly, because of masking by the embankments, the headscarps for both LS-Emb-S and LS-Emb-N can no longer be identified clearly, and therefore head scarp slope gradients and minimum water depths could not be ascertained.

Table 2. *Interpreted areas and volumes (based on estimated surface change) of the northern and southern embankments, and estimated volume of soft organic soil upon which the embankments were placed*

	Northern embankment	Southern embankment
Interpreted embankment area* (m^2)	3880	3850
Calculated net volume (m^3)	6300	13800
Interpreted area of organic soil at surface within embankment area† (m^2)	3090	2580
Estimated potential volume of soft organic material that could be displaced‡ (m^3)	8500	7100

*The interpreted area includes only loch bed shown within the multibeam data (minimum water depth of *c.* 4 m).
†The area of organic soil at surface was delimited based on pre-embankment borehole information and interpretation of the surrounding geomorphology.
‡The estimated potential volume of soft organic material is based on a mean surface organic thickness (2.75 m) from the two boreholes within the southern embankment area.

beneath the loch bed. Along the shore the alluvial fan areas are characterized by thicker sand and gravel units with some surface and buried layers of soft organic soil. However, further downslope, and between the fans, the organic soil is present at the loch bed surface (this interpretation differs slightly from the original ground model suggested by Howison and MacDonald (1988); see discussion section). The sequence of soil units likely to have been subjected to loading by the embankments is shown in the short perpendicular (west–east) cross-sections. Assuming the surface organic layer thickness in the boreholes is representative, a crude estimation was made of the volume of organic soil below each embankment (Table 2).

The estimated depth of net erosion and deposition or thickening resulting from the embankment placement and associated landslides (LS-Emb-N, LS-Emb-S and LS-Mor) is shown in Figure 12. Apparent volumes associated with different segments of the landslides are also given. We note, however, that there is considerable uncertainty associated with these estimates, especially in areas where previous landslide activity may have affected the topography (such as the site of the overridden LS-Fn landslide lobe). Nonetheless, the plot does give a general impression of locations where erosion and deposition were focused. Areas of elevation gain arising from the final embankment construction are clearly shown. This generally amounts to 4.0–5.0 m or more at the southern embankment and 2.0–3.0 m at the northern embankment. Howison and MacDonald (1988) reported that the major displacement at the southern embankment took place when it was near completion, with some 15 000 m^3 rock fill moving downslope. The elevation gain shown at the southern embankment in Figure 12 may be considered representative of the volume of rock fill that was displaced during the first phase of construction, prior to failure. Indeed, the embankment volume calculated using the difference between the modern bathymetry and the estimated pre-embankment surface is 13 800 m^3 (Table 2), which is very similar to the volume given by Howison and MacDonald (1988).

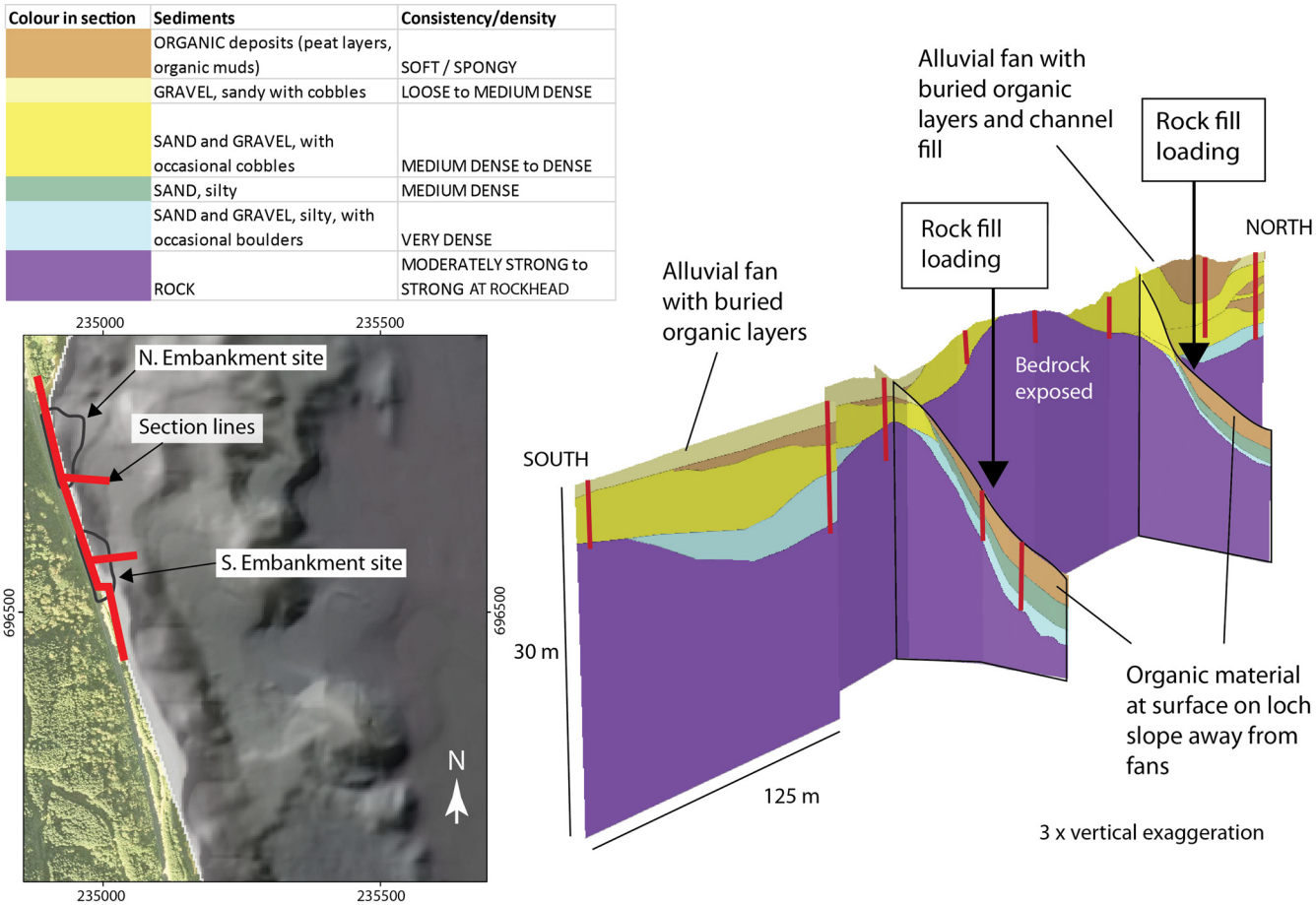

Fig. 11. Interpolated pre-embankment surface and fence diagram with simplified pre-embankment geology in the head scarp areas. Red lines in fence diagram give approximate borehole positions. Aerial photograph © Getmapping: Licence Number UKP2006/01.

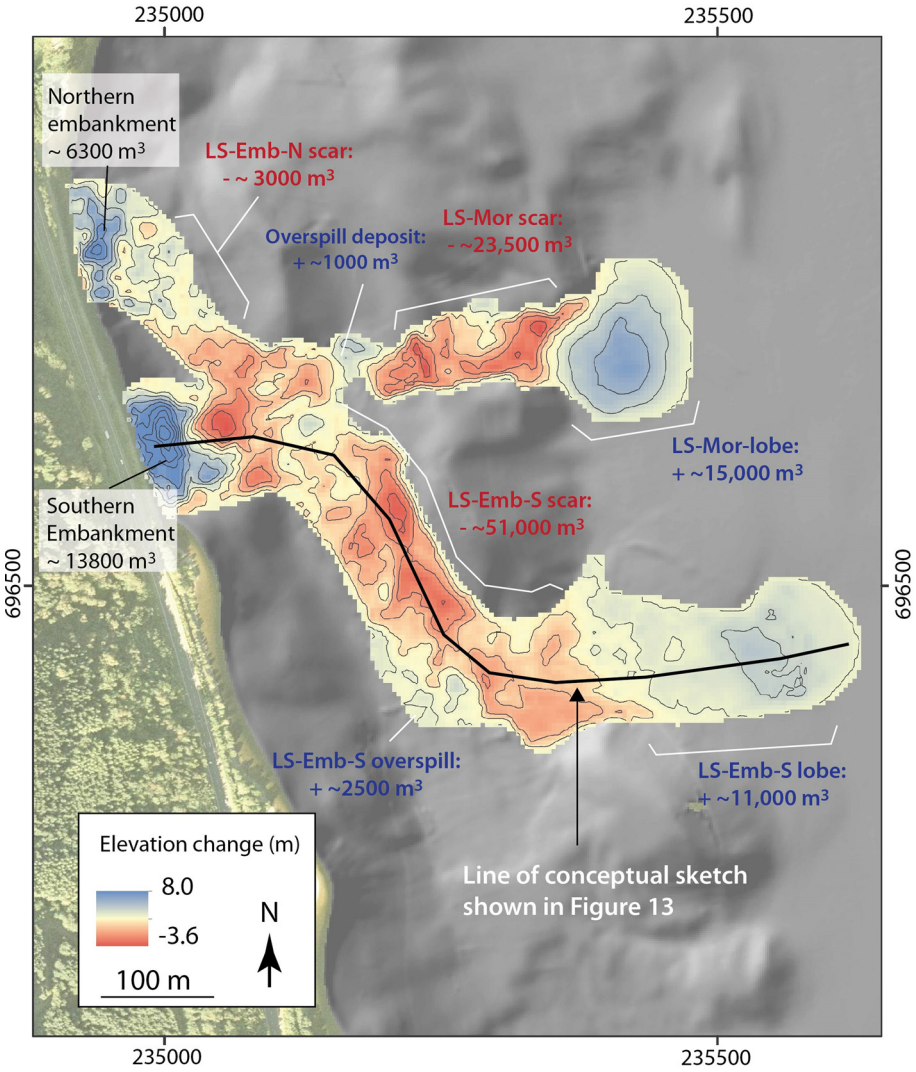

Fig. 12. Estimated elevation change showing areas of embankment placement and sediment deposition or thickening (blue) and erosion (red). The line of the conceptual sketch in Figure 13 is shown. Aerial photograph © Getmapping: Licence Number UKP2006/01.

Elevation gains are also evident at the depositional lobes and above the headscarp of the moraine landslide (LS-Mor) where debris from one (or both) of the embankment landslides appears to have overtopped the ridge. The main erosional areas (locally up to 3.6 m) appear to be immediately below the southern embankment (where backscatter data are interpreted to suggest erosion down to bedrock), near the eastern edge of the LS-Emb-S landslide 'channel' and in the LS-Mor landslide scar area.

Overall, net erosion from the southern embankment and moraine landslide scar areas is approximated to be *c.* 74 500 m^3. The displacement of the southern embankment included a possible rockfill volume of 13 800 m^3 and potentially up to 7100 m^3 of organic soil upon which the fill was placed (Table 2). This gives an approximate total entrainment volume of up to *c.* 95 400 m^3. The total volume of deposition that could be identified in the multibeam (lobes and overspill areas) is *c.* 30 000 m^3. This is lower than the estimated entrainment volume and may be explained by (1) compression of soil within, and possibly beyond, the visible depositional lobes (this is supported by observation of compressional ridges), (2) possible loss of fine soil to suspension or settling of material that is not detectable in the resolution of our datasets and (3) uncertainty in the estimation of the pre-landslide bathymetric surface.

Interpreting the type of subaqueous landslide associated with the southern embankment (LS-Emb-S)

The nature of the displacement at the embankment landslides is difficult to classify without core data to validate the deformation observed in the autochthonous and allochthonous soils, and because the final embankments now cover the original headscarp zones. However, based on the morphology, original boreholes and the available seismic data, the following interpretations may be inferred for the southern embankment landslide (LS-Emb-S), for which we have the most information (Fig. 13).

Boreholes suggest the presence of cohesive material (organic silt and clay) overlying a dense, more granular and non-cohesive layer on the nearshore slope (Fig. 11). Distinct scars with side scarps and a shallow (although undulating) failure surface are consistent with features attributable to sliding, where shear failure was focused at the base of the mass movement; in this case within the organic soil upon which the embankment fill was placed. However, the boulder fill (estimated by Howison and MacDonald (1988) to have been 15 000 m^3) would also have formed part of the moving material and may not necessarily have moved as a coherent block. The depth of erosion and interpreted exposure of bedrock in the scar area immediately below the southern embankment (Figs 5, 12 and 13) also suggest that the granular soils below the organic layer became incorporated within the event immediately downslope from the embankment, with potential for more flow-like behaviour (see Mulder and Cochonat 1996). We also note that both initial placement of the rock fill (and mass transport of the rock fill) onto the lower gradient nearshore slope is likely to have had the effect of rapidly increasing pore fluid pressures in the underlying soil unit, potentially influencing the triggering of motion. Such an effect is considered to lie within the gravity flow and mass flow classification as outlined in the Mulder and Cochonat (1996) scheme.

Evidence for movement as, or rapid transition to, mass flow also includes possible overtopping of the side scarp in the bend of the LS-Emb-S landslide and the overall channelized form of the landslide (focused between the moraine and nearshore slope). In addition, the chaotic to transparent seismic units in the upslope side of the depositional zones may indicate loss of prefailure stratigraphy owing to a higher degree of remoulding and dilation with shear failure being distributed through the mass, such as in flow processes associated with debris flows (e.g. Schnellmann *et al.* 2005; Sammartini 2021).

However, compressional ridges are evident towards the distal edges of the depositional lobe, suggesting that the landslide became frontally confined and did not ramp up to move further across the loch floor (e.g. Frey-Martínez *et al.* 2006; Clare *et al.* 2019; Strupler *et al.* 2019). The Holocene loch bed muds would be expected to increase in thickness from the nearshore slope to the loch floor, and this transition may therefore have been accompanied by a return to more cohesive movement in the landslide as the base of the failure moved back up into finer grained soil (Fig. 13). We note, however, that there is some uncertainty over the nature of the material in the region of the pre-existing LS-Fn landslide lobe that the southern embankment landslide partially overrides.

Runout modelling for the southern embankment subaqueous landslide (LS-Emb-S)

Runout modelling for the southern embankment (LS-Emb-S) landslide was informed by the conceptual model described above and used the estimated pre-embankment loch bed surface (Fig. 11) as an initial condition. The initial volume was implemented using a release block approach, based on the total volume (20 900 m^3) of estimated embankment fill and the directly underlying organic soil (Table 2), and assuming instantaneous failure at source. Preliminary modelling was carried out to back-calibrate the rheological and entrainment parameters by best fitting interpretations of runout pattern and distance, erosion and deposition depth, and deposition pattern from the observation datasets. The area of the moraine landslide (LS-Mor) was also included within the model domain to allow for any overspill in that area. Based on geomorphological interpretations, a total entrained volume (including initial volume) of 100 000 m^3 was used for the modelling. A parametric sensitivity analysis of rheological parameters on eroded volume was carried out in this study by keeping entrainment parameters constant. The results imply a greater control of friction coefficient on entrained volume than the turbulence coefficient.

An initial set of calibration trials that considered a single rheological domain for the entire landslide footprint produced a runout extending beyond the interpreted limit and did not match observed characteristics such as erosion depth and deposition pattern. Therefore, an attempt was made to better capture the interpreted evolution of the landslide (illustrated schematically in Fig. 13) by considering two rheological domains, through the application of the Voellmy-frictional (where basal shear occurs in dense granular material) and Voellmy-cohesion (where the basal shear zone transitions to loch bed muds) models. This systematic adjustment underpinned by observations provided a good fit to the landslide runout, erosion and deposition morphology, and the best-fit rheological parameters are as shown in Table 3. A flow stopping threshold (based on comparing the momentum values of all grid cells with the maximum momentum sum) of 7% was used and was informed by 34 trials whereby too large a threshold resulted in early stopping and too small a value resulted in slow creeping and velocity oscillations. This threshold value also aligns with the recommendation of <10% in the model guidance (RAMMS 2017).

Figure 14 illustrates the simulated mass flow to take 2750 s (*c.* 45 min) to progress from initiation to final deposition at the stopping criterion of 7%. The combined rockfill and organic soil volume of 20 933 m^3 upon failure has its substantial mass routed through the SSW-trending channel, whereas a small amount of material breaks away and has enough energy to overtop the moraine (Fig. 14b). At 300 s, the debris flow mass upslope starts to elongate such that a thin mass with a depth of <1 m separates out and flows ahead of the main volume. The mass flow reaches the southern channel bend at 600 s (Fig. 14c) with an estimated maximum velocity of 1.8 m s^{-1} (Fig. 14d) and erodes to a depth of about 2 m around the bend (Fig. 14f). The distinct surges seen within the velocity profile after 600 s at point A in Figure 14e signify the continued downslope movement of residual debris material after the initial front has passed through. Further in time the mass flow front exits the channel and flows into the lower gradient loch bed between the eastern moraine edge and the older LS-Fn landslide deposit. Some material is diverted NE around the existing LS-Fn landslide lobe, whereas the remainder travels out from the mass flow front and carries on eastwards over the older deposit, before forming a depositional lobe within the thicker Holocene loch bed muds (Fig. 14d).

Maximum erosion depth in the simulated landslide occurs immediately downslope from the embankment and is consistent with the area where backscatter data and the interpretation of possible dykes suggest erosion down through the granular layer to the bedrock surface (compare Figs 5, 12 and 14f). The focused erosion in the SE-trending channel on the shoreward side of the moraine ridge is also broadly consistent with estimated patterns of surface change from the geomorphological analysis (e.g. Figs 6, 12 and 14f). The simulation indicates some debris flow mass

Table 3. *Calibrated parameters for RAMMS modelling*

Parameters	Calibrated values
Voellmy-friction: wider loch bed surface	
Friction coefficient	0.04
Turbulence coefficient	200
Voellmy-friction: runout and entrainment zone where base of landslide occurs in dense granular material	
Friction coefficient	0.4
Turbulence coefficient	150
Voellmy-cohesion: deposition zone where base of landslide occurs in loch muds	
Yield strength (Pa)	20
Hardening parameter	2.5
Turbulence coefficient	100
Entrainment parameters	
Erosion rate (m s^{-1})	0.0125
Potential erosion depth (m)	0.1
Critical shear stress (kPa)	1.5

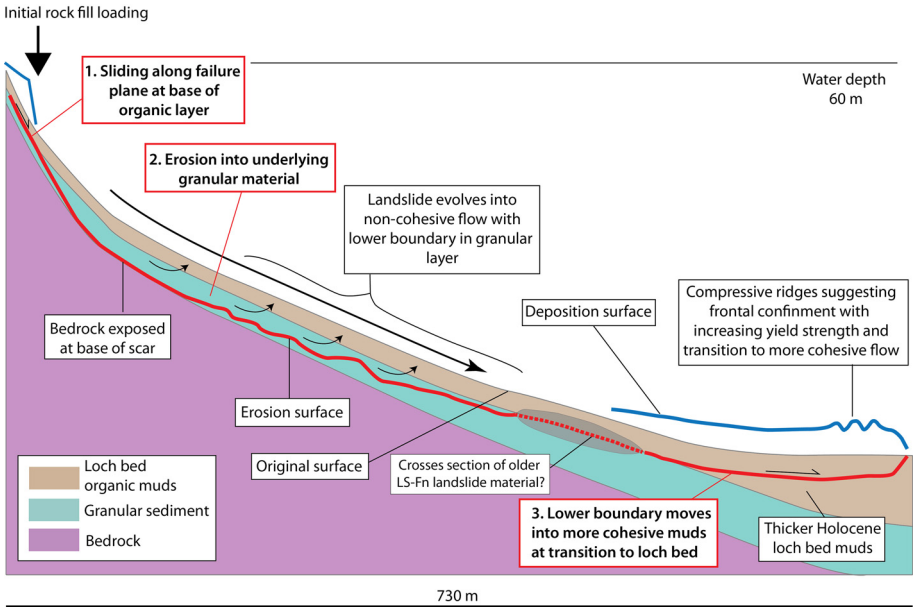

Fig. 13. Conceptual sketch illustrating the interpretation of the southern embankment subaqueous landslide, LS-Emb-S.

overtopping the moraine ridge and subsequent entrainment producing the moraine (LS-Mor) landslide. However, the simulated erosion depths and deposit height are not as large as indicated by observations. It may therefore be possible that the northern embankment landslide (LS-Emb-N), which has not been included in the modelling, had also affected this area, initiating some of the erosion of the LS-Mor landslide scar.

Discussion

Subaqueous landslides have been linked to anthropogenic activity (embankment fillings and construction works) at a small number of locations within fjord settings in Norway (e.g. L'Heureux *et al.* 2010; Vardy *et al.* 2012). At Holy Loch in Scotland, Carter *et al.* (2020) suggested that a shallow translational failure may have been related to clean-up activities following decades of naval use, and Fielding *et al.* (2018) highlighted that dredging may have played a role in slope destabilization at the Trout Beck delta fan in Lake Windermere. The Wades Bridge Bank site described here provides a clear example of subaqueous landslides associated with placement of embankment fill in a steep lochside (fjord) setting. It therefore adds to our understanding of the interaction between shoreline infrastructure and subaqueous slopes in these types of environments.

The datasets investigated here allow new interpretations of the subaqueous landscape at the Wades Bridge Bank site (Fig. 3), which can be used to build on the conceptual model developed in the original investigation at the site (Howison and MacDonald 1988). For example, the mapped distribution and extent of shoreline alluvial fans provides additional context for the interpretation of the site investigation boreholes and probable soil sequence. In this study, we suggest that the observations of buried organic fine-grained soil beneath sand and gravel are more likely to be associated with the alluvial fans (locally undergoing active reworking or pulses of sedimentation) and may be locally restricted, whereas further from the fans, and between the fans, the organic silts are more likely to rest at the surface (Fig. 11). This interpretation differs from the original design whereby the organic silts were assumed to be buried below sand and gravel at the embankment sites, with displacement considered unlikely to occur (Howison and MacDonald 1988).

The data also clearly illustrate the (previously unknown) spatial extent of landslide activity resulting from the embankments on the loch bed landscape. The only significant displacement reported at the time of construction was the 15 000 m^3 downslope movement of fill at the southern embankment. However, the interpretation here based on new multibeam and seismic data suggests that landslide activity occurred at the northern embankment (LS-Emb-N), southern embankment (LS-Emb-S) and the eastern moraine slope (LS-Mor). The largest of these, the LS-Emb-S landslide, was 'channelled' along the nearshore side of the moraine ridge and travelled some 700 m (Table 1), crossing approximately one-third of the width of Loch Lomond in this area. The Wades Bridge Bank subaqueous landslides have 'height fall' to horizontal runout ratios of between 0.07 and 0.09, with volumes of an order of magnitude that plot towards the left side of the threshold charts of Hampton *et al.* (1996) and De Blasio *et al.* (2006) and below the subaerial landslide limit, highlighting their high mobility characteristics. The morphometric parameters (Table 1) and estimated volumes of the embankment landslides are comparable with several natural subaqueous landslides in fjord or loch environments around the western Scottish coastline that were described by Carter *et al.* (2020) as 'singular slumps' and ranged between 20 000 and 100 000 m^3 (estimated using the same method as in this paper). They are, however, somewhat smaller (and narrower) than the 'multiple single-type' mass movements identified in that study, which reached up to 500 000 m^3. Lowag *et al.* (2012) have also presented volumes of between 2100 and >100 000 m^3 for 17 mass movement deposits identified using densely spaced seismic reflection profiles from Lake Windermere in England's Lake District. The estimated volumes from the Wades Bridge Bank embankment landslides fall within that range. The Wades Bridge Bank subaqueous landslides appear to be significantly larger than recorded recent onshore sediment failures in this part of the Scottish Highlands. As a comparison, Bainbridge *et al.* (2022) estimated a total volume of source areas for all subaerial debris flows and debris falls between 2003 and 2020 at the nearby Rest and Be Thankful site to be *c.* 5400 m^3, an order of magnitude smaller than the estimated entrained volume of up to 94 500 m^3 from the Wades Bridge Bank subaqueous landslides event.

An important observation from the Wades Bridge Bank site is the evidence for older Holocene landslides. One such example is the fan edge landslide (LS-Fn), which is similar in scale to the embankment landslides (Table 1) and was also potentially linked to loading of the soil units on the loch slope (in this instance, loading by material fed from the alluvial fan above). Stacked debris flow units identified in the seismic data (Fig. 8) indicate that lobes from the embankment

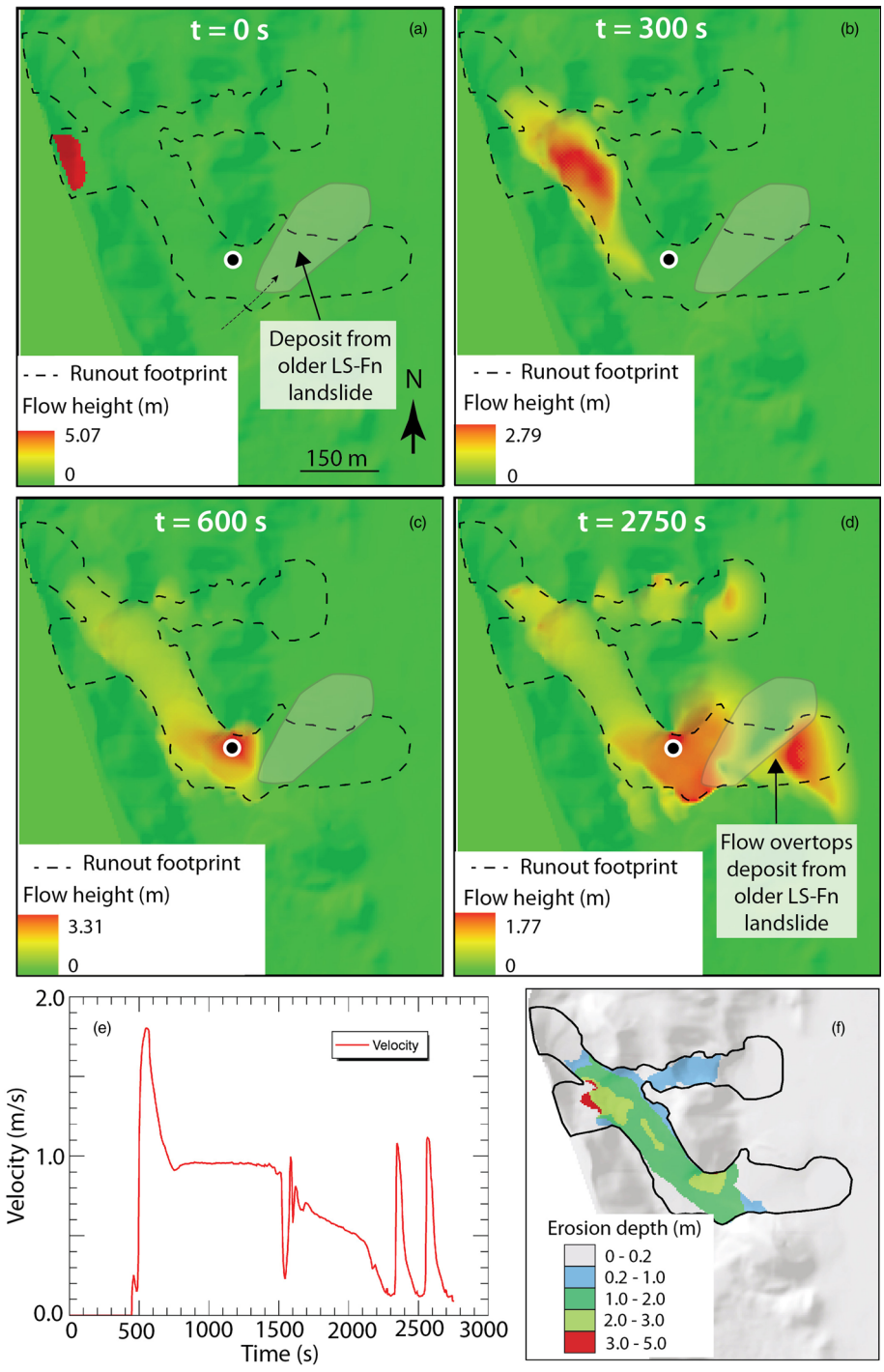

Fig. 14. (**a**–**d**) Subaqueous landslide propagation and flow height distribution for LS-Emb-S at the following timesteps: (**a**) initial time ($t = 0$); (**b**) $t = 300$ s; (**c**) $t = 600$ s; (**d**) $t = 2750$ s. (**e**) Modelled velocity at the point marked by the black circle in (**a**)–(**d**) through the duration of the LS-Emb-S landslide. (**f**) Modelled erosion of loch bed material owing to southern embankment landslide, LS-Emb-S.

landslides were deposited in similar locations to debris deposited during earlier Holocene landslide activity. Although these data were not available at the time of the original investigation, they collectively provide evidence about the nature and pattern of pre-existing subaqueous landslide susceptibility, showing the value of detailed site surveys in modern investigations.

The runout modelling presented in this paper is based largely on parameterization guided by interpretations from the geomorphological analysis, original (pre-embankment) investigation boreholes and the description given by Howison and MacDonald (1988). The resulting simulation shows a good fit to the interpreted embankment landslide extent and erosion and deposition patterns, and provides an illustration of possible velocities, flow heights and durations. The deposition of the flow onto the loch bed may have been triggered by a reduction in slope angle from 4° to <0.5° and the cohesive nature of the flow (calibrated to a yield strength of 20 Pa). However, the model underpredicts the depth of the depositional lobe compared with that estimated from the seismic data, one of the reasons for which might be the limited ability of the RAMMS model to simulate the process of debris material compression at deposition. The erosion process modelled in this study aligns with the excavation-based type II erosion (Mitchener and Torfs 1996; Amos *et al.* 1997; Talling *et al.* 2002) in which the critical shear stress remains constant across the depth. However, the calibrated critical shear value of 1.5 kPa for erosion is about three to four orders of magnitude higher than the experimental values summarized in the study by Talling *et al.* (2002), which may be scaling-related. The current parameterization using the Voellmy-type rheology is a preliminary effort to model the subaqueous process and it is recognized that opportunities for further refinement with improved input data and exploration of alternative (e.g. multiphase) models integrating physical soil properties exist.

There is currently only a very small dataset for nearshore landslides in steep UK coastal and inland waterbodies (Carter *et al.* 2020). Increasing shoreline development such as transport infrastructure improvement (road, rail), tourism (waterfront development), aquaculture installations (fish farms) and energy (cable landfall sites from offshore wind or potential for floating solar) will require a greater understanding of these environments and possible impacts from loading on nearshore slopes. Subaqueous landslides have potential to generate destructive waves or damage subaqueous infrastructure (pipelines or cables). Therefore, it is valuable to continue to document the nature and extent of past failures where there is strong evidence linking events to shoreline development in order to further understanding of these environments. The larger the database, the more statistically robust any analysis carried out on these known subaqueous failures will be, and continued research and documentation is crucial for this purpose. The research in this paper illustrates the value of offshore geophysical datasets in understanding the landscape context at shorelines in steep glaciated environments. Integrating these data as part of a combined onshore and offshore approach has clear potential benefit for investigations where future infrastructure developments are planned in such terrain.

Conclusions

- Two deepwater embankments were constructed on the shoreline of Loch Lomond at Wades Bridge Bank as part of the A82 road improvement in the 1980s. During construction, a significant displacement was reported at the southern embankment prior to stabilization and completion. New multibeam and seismic data collected *c.* 20 years after the embankment completion provide evidence for three subaqueous landslides, likely to have been associated with loch slope loading by embankment fill and displacements at the time of construction.
- The total volume of material entrained by the embankment landslides, including the fill material from the southern embankment, is estimated to have been up to 95 000 m^3. The largest landslide, associated with the southern embankment displacement, travelled more than 700 m, approximately one-third of the distance across Loch Lomond.
- Interpretations of the bathymetric and seismic data indicate the occurrence of several earlier Holocene subaqueous landslides in the area. At least one of these earlier landslides was of a similar size to the embankment landslides, and deposits were focused in similar areas. The interpretations suggest a pre-existing landslide susceptibility in the vicinity of the site, indicating the clear value of multibeam and seismic datasets in these environments.
- Interpretation of boreholes and multibeam data indicate the presence of soft organic soil on the loch slopes. The organic material appears to be buried by granular soils in the vicinity of nearby alluvial fans, as indicated by boreholes. However, the interpretation in this study is that the organic soil was likely to be present at surface further away from the fans, in locations that were subjected to loading by the embankments. This interpretation differs from the original ground model but is informed by further understanding of the geomorphological context provided by the new data.
- A landslide runout simulation was developed, which fits with the observed patterns of erosion and deposition seen for the southern embankment subaqueous landslide. The model suggests that the flow took *c.* 45 min to progress from initiation to final deposition, with maximum velocities of *c.* 2 m s^{-1}.
- There is currently only a small dataset for nearshore subaqueous landslides in steep coastal inland waterbodies. Increasing demands from shoreline development will require a greater understanding of these environments. Documentation of interactions between historical shoreline infrastructure and steep nearshore subaqueous slopes can potentially support this understanding.
- Integrating high-resolution bathymetry and shallow sub-bottom seismic imaging with onshore investigations can be a valuable approach when investigating the landscape context for future shoreline infrastructure development in steep glaciated terrain.

Scientific editing by Colin Serridge; Michael Davies

Acknowledgements The 2007–2008 multibeam survey of Loch Lomond was undertaken in partnership with the Loch Lomond and Trossachs National Park (LLTNP) using their boat, the *Bata Greine*, for which LLTNP is thanked. E. Phillips is thanked for discussions on aspects of this work and for reviewing an earlier version of the paper. We are grateful to the journal reviewers, J. Bull and A. Hart, for their constructive comments, which improved this paper. This work is published with the permission of the Executive Director of the British Geological Survey (UKRI).

Author contributions **AF**: conceptualization (lead), investigation (equal), project administration (lead), writing – original draft (lead), writing – review & editing (equal); **NN-V**: investigation (equal), writing – original draft (supporting), writing – review & editing (equal); **GC**: conceptualization (supporting), investigation (equal), writing – review & editing (equal); **ND**: investigation (equal), writing – review & editing (equal); **RC**: data curation (lead), resources (lead)

Funding This work was supported by the BGS via NERC National Capability.

Competing interests The authors declare that they have no known competing financial interests or personal relationships that could have appeared to influence the work reported in this paper.

Data availability The datasets analysed during the current study are available from the British Geological Survey upon request. In due course they will be made accessible through the National Geoscience Data Centre (https://www.bgs.ac.uk/geological-data/national-geoscience-data-centre/).

References

Amos, C.L., Feeney, T., Sutherland, T.F. and Luternauer, J.L. 1997. The stability of fine-grained sediments from the Fraser River Delta. *Estuarine, Coastal and Shelf Science*, **45**, 507–524, https://doi.org/10.1006/ecss.1996.0193

Bainbridge, R., Lim, M. *et al.* 2022. Detection and forecasting of shallow landslides: lessons from a natural laboratory. *Geomatics, Natural Hazards and Risk*, **13**, 686–704, https://doi.org/10.1080/19475705.2022.2041108

Berger, C., McArdell, B.W. and Schlunegger, F. 2011. Direct measurement of channel erosion by debris flows, Illgraben, Switzerland. *Journal of Geophysical Research*, **116**, F01002, https://doi.org/10.1029/2010JF001722

BGS 1987. *Ben Lomond. Scotland Sheet 38W. Solid. 1:50,000 Geological Map Series*. British Geological Survey, Keyworth, Nottingham.

Carter, G.D., Cooper, R., Gafeira, J., Howe, J.A. and Long, D. 2020. Morphology of small-scale submarine mass movement events across the northwest United Kingdom. *Geomorphology*, **365**, 107282, https://doi.org/10.1016/j.geomorph.2020.107282

Chiocci, F.L., Cattaneo, A. and Urgeles, R. 2011. Seafloor mapping for geohazard assessment: state of the art. *Marine Geophysical Research*, **32**, 1–11, https://doi.org/10.1007/s11001-011-9139-8

Christen, M., Kowalski, J. and Bartelt, P. 2010. RAMMS: Numerical simulation of dense snow avalanches in three-dimensional terrain. *Cold Regions Science and Technology*, **63**, 1–14, https://doi.org/10.1016/j.coldregions.2010.04.005

Clare, M., Chaytor, J. *et al.* 2019. A consistent global approach for the morphometric characterization of subaqueous landslides. *Geological Society, London, Special Publications*, **477**, 455–477, https://doi.org/10.1144/SP477.15

De Blasio, F.V., Elverhoi, A., Engvik, L., Issler, D., Gauer, P. and Harbitz, C. 2006. Understanding the high mobility of subaqueous debris flows. *Norwegian Journal of Geology*, **86**, 275–284.

Dickson, J.H., Stewart, D.A., Thompson, R., Turner, G., Baxter, M.S., Drndarsky, N.D. and Rose, J. 1978. Palynology, palaeomagnetism and

radiometric dating of Flandrian marine and freshwater sediments of Loch Lomond. *Nature*, **274**, 548–553, https://doi.org/10.1038/274548a0

Farmer, J.G. and Lovell, M.A. 1986. Natural enrichment of arsenic in Loch Lomond sediments. *Geochimica et Cosmochimica Acta*, **50**, 2059–2067, https://doi.org/10.1016/0016-7037(86)90259-0

Fielding, J.J., Kemp, A.E.S. *et al.* 2018. Palaeoseismology from microfabric and geochemical analysis of lacustrine sediments, Windermere, UK. *Journal of the Geological Society, London*, **175**, 903–914, https://doi.org/10.1144/jgs2017-094

Frank, F., McArdell, B.W., Oggier, N., Baer, P., Christen, M. and Vieli, A. 2017. Debris-flow modeling at Meretschibach and Bondasca catchments, Switzerland: sensitivity testing of field-data-based entrainment model. *Natural Hazards and Earth System Sciences*, **17**, 801–815, https://doi.org/10.5194/nhess-17-801-2017

Frey-Martínez, J., Cartwright, J. and James, D. 2006. Frontally confined versus frontally emergent submarine landslides: A 3D seismic characterisation. *Marine and Petroleum Geology*, **23**, 585–604, https://doi.org/10.1016/j.marpetgeo.2006.04.002

Hampton, M.A., Lee, H.J. and Locat, J. 1996. Submarine landslides. *Reviews of Geophysics*, **34**, 33–59, https://doi.org/10.1029/95RG03287

Hansom, J.D. and McGlashan, D.J. 2000. *Impacts of Bank Protection on Loch Lomond*. Scottish Natural Heritage Research, Survey and Monitoring Report, **154**.

Hough, G., Green, J., Fish, P., Mills, A. and Moore, R. 2011. A geomorphological mapping approach for the assessment of seabed geohazards and risk. *Marine Geophysical Research*, **32**, 151–162, https://doi.org/10.1007/s11001-010-9111-z

Howison, J.A. and MacDonald, A. 1988. Trunk Road A82: Loch Lomondside road: conception to implementation. *Proceedings of the Institution of Civil Engineers*, **84**, 497–518, https://doi.org/10.1680/iicep.1988.32

Howison, J. and MacDonald, A. 1989. Discussion: Trunk Road A82: the Loch Lomondside road: conception to implementation. *Proceedings of the Institution of Civil Engineers*, **86**, 963–971, https://doi.org/10.1680/iicep.1989.3168

L'Heureux, J.S., Hansen, L., Longva, O., Emdal, A. and Grande, L. 2010. A multidisciplinary study of submarine landslides at the Nidelva fjord delta, Central Norway – implications for geohazard assessment. *Norwegian Journal of Geology*, **90**, 1–20.

Lowag, J., Bull, J.M., Vardy, M.E., Miller, H. and Pinson, L.J.W. 2012. High-resolution seismic imaging of a Younger Dryas and Holocene mass movement complex in glacial lake Windermere, UK. *Geomorphology*, **171–172**, 42–57, https://doi.org/10.1016/j.geomorph.2012.05.002

MacLeod, A., Palmer, A., Lowe, J., Rose, J., Bryant, C. and Merritt, J. 2011. Timing of glacier response to Younger Dryas climatic cooling in Scotland. *Global and Planetary Change*, **79**, 264–274, https://doi.org/10.1016/j.gloplacha.2010.07.006

Miller, H., Bull, J.M., Cotterill, C.J., Dix, J.K., Winfield, I.J., Kemp, A.E. and Pearce, R.B. 2013. Lake bed geomorphology and sedimentary processes in glacial lake Windermere, UK. *Journal of Maps*, **9**, 299–312, https://doi.org/10.1080/17445647.2013.780986

Mitchener, H. and Torfs, H. 1996. Erosion of mud/sand mixtures. *Coastal Engineering*, **29**, 1–25, https://doi.org/10.1016/S0378-3839(96)00002-6

Mulder, T. and Cochonat, P. 1996. Classification of offshore mass movements. *Journal of Sedimentary Research*, **66**, 43–57, https://doi.org/10.1306/D42682AC-2B26-11D7-8648000102C1865D

Pinson, L.J., Vardy, M.E., Dix, J.K., Henstock, T.J., Bull, J.M. and Maclachlan, S.E. 2013. Deglacial history of glacial lake Windermere, UK: implications for the central British and Irish Ice Sheet. *Journal of Quaternary Science*, **28**, 83–94, https://doi.org/10.1002/jqs.2595

RAMMS 2017. *RAMMS: DEBRIS FLOW User Manual*. ETH, Davos, https://ramms.slf.ch/ramms/downloads/RAMMS_DBF_Manual.pdf

Rose, J., Lowe, J.J. and Switsur, R.V. 1988. A radiocarbon date on plant detritus beneath till from the type area of the Loch Lomond Readvance. *Scottish Journal of Geology*, **24**, 113–124, https://doi.org/10.1144/sjg24020113

Sammartini, M., Moernaut, J., Kopf, A., Stegmann, S., Fabbri, S.C., Anselmetti, F.S. and Strasser, M. 2021. Propagation of frontally confined subaqueous landslides: Insights from combining geophysical, sedimentological, and geotechnical analysis. *Sedimentary Geology*, **416**, 105877, https://doi.org/10.1016/j.sedgeo.2021.105877

Schnellmann, M., Anselmetti, F.S., Giardini, D. and McKenzie, J.A. 2005. Mass movement-induced fold-and-thrust belt structures in unconsolidated sediments in Lake Lucerne (Switzerland). *Sedimentology*, **52**, 271–289. https://doi.org/10.1111/j.1365-3091.2004.00694.x

Schürch, P., Densmore, A.L., Rosser, N.J. and McArdell, B.W. 2011. Dynamic controls on erosion and deposition on debris-flow fans. *Geology*, **39**, 827–830, https://doi.org/10.1130/G32103.1

SEPA 2022. SEPA Water level data. Loch Lomond @ Ross Priory, https://www2.sepa.org.uk/waterlevels/default.aspx?sd=t&lc=133124 [last accessed 16 February 2022].

Stephenson, D. and Gould, D. 1995. *British Regional Geology: The Grampian Highlands*, 4th edn. Reprint 2007. British Geological Survey, Keyworth, Nottingham.

Stoker, M.S., Wilson, C.R., Howe, J.A., Bradwell, T. and Long, D. 2010. Paraglacial slope instability in Scottish fjords: examples from Little Loch Broom, NW Scotland. *Geological Society, London, Special Publications*, **344**, 225–242, https://doi.org/10.1144/SP344.16

Strupler, M., Anselmetti, F.S., Hilbe, M. and Strasser, M. 2019. Quantitative characterization of subaqueous landslides in Lake Zurich (Switzerland) based on a high-resolution bathymetric dataset. *Geological Society, London, Special Publications*, **477**, 399–412, https://doi.org/10.1144/SP477.7

Talling, P.J., Peakall, J. *et al.* 2002. Experimental constrains on shear mixing rates and processes: implications for the dilution of submarine debris flows. *Geological Society, London, Special Publications*, **203**, 89–103, https://doi.org/10.1144/SP477.7

Transport Scotland 2009. *Strategic Transport Projects Review: Final Report*.

Transport Scotland 2016. *Road Asset Management Plan for Scottish Trunk Roads*.

Turner, G.M. and Thompson, R. 1979. Behaviour of the Earth's magnetic field as recorded in the sediment of Loch Lomond. *Earth and Planetary Science Letters*, **42**, 412–426, https://doi.org/10.1016/0012-821X(79)90050-5

Vardy, M.E., L'Heureux, J.S. *et al.* 2012. Multidisciplinary investigation of a shallow near-shore landslide, Finneidfjord, Norway. *Near Surface Geophysics*, **10**, 267–277, https://doi.org/10.3997/1873-2012022